Intelligent Control Algorithm for Clean Heating Temperature Based on Optical Fiber Grating Temperature Sensors

Shuang Li*, Lin Zhu, Yu Zhang

School of Energy and Environmental Engineering, Jilin University of Architecture and Technology, Changchun 130114, China

*Corresponding author: Shuang Li; Email: lishuang22@imte.ac.cn

Abstract: This paper proposes an intelligent control algorithm based on fiber Bragg grating temperature sensors to address the problems of inaccurate temperature measurement caused by electromagnetic interference in traditional temperature sensors in geothermal clean heating systems, poor adaptability of conventional PID controllers to complex and variable working conditions, and large control overshoot. This algorithm uses fiber Bragg grating sensors to construct a time-division multiplexing sensing network, which utilizes its anti electromagnetic interference characteristics and the linear relationship between temperature and wavelength to solve the problem of accurate temperature measurement in complex geothermal heating environments, providing real-time and reliable data for temperature control. In terms of control indicators, time squared multiplied by absolute error integral is used instead of traditional absolute error integral to adapt to conditions with variable parameters. At the same time, the BP neural network is introduced to perform online adaptive tuning of the proportional, integral, and derivative parameters of the PID controller, enabling the controller to automatically adjust control parameters based on the real-time operating status of the system, and improve its response capability to complex working conditions such as sudden changes in thermal load and outdoor temperature. The experimental results show that under high interference levels, the sensor network can still stably transmit 20 data packets within 100 seconds. Compared with existing methods based on wireless temperature sensors, thermocouple sensors, and model predictive control, the control overshoot of this algorithm is reduced to 8%, and the adjustment time is shortened to 10.2 minutes. During the 24-hour continuous operation test, when the outdoor temperature fluctuated within the range of 5 ℃ to 12 ℃, the indoor temperature remained stable at around 25 ℃ without any noticeable fluctuations. This algorithm provides a temperature control scheme for geothermal clean heating with anti-interference ability, adaptive adjustment ability, and high-precision control performance.

Keywords: Optical fiber grating; Temperature sensor; Sensor network; Geothermal energy; Intelligent control; PID controller; BP neural network

This provisional PDF is the accepted version. The article should be cited as: J. Eur. Opt. Society-Rapid Publ., https://doi.org/10.1051/jeos/2026054

1 Introduction

Geothermal energy, as a highly promising renewable energy source [1], is gradually emerging in the heating sector. Geothermal clean heating [2] refers to the utilization of thermal energy stored within the Earth, through a series of technical means such as geothermal well extraction and heat exchange, to convert geothermal energy into heat for indoor heating of buildings, thus achieving a method of winter heating [3]. Compared to traditional heating methods such as coal and oil, geothermal clean heating has many significant advantages [4]. It not only effectively reduces greenhouse gas emissions and minimizes pollution to the atmosphere, aligning with the environmentally friendly concept of sustainable development, but also provides relatively stable energy supply that is not affected by fluctuations in fuel market prices, ensuring reliable heating [5].

However, to fully leverage the advantages of geothermal clean heating, precise and intelligent temperature control is crucial. Geothermal heating systems involve multiple complex components, including geothermal wells, heat exchange stations, heating pipelines, and indoor terminal heating devices, with temperature variations in each component being interrelated yet unique [6]. On one hand, reasonable temperature control can ensure that indoor temperatures remain within a comfortable range for humans, preventing excessive heat or cold, thereby enhancing the quality of life for residents. For instance, on a cold winter day, precise temperature regulation can keep the indoors warm and spring-like, protecting people from the cold. On the other hand, effective temperature control can optimize the utilization efficiency of geothermal energy, preventing excessive waste of heat or insufficient supply [7]. By monitoring in real-time and adjusting dynamically, the heating system can operate flexibly according to factors such as outdoor temperature changes and building heat load demands, maximizing the effectiveness of geothermal energy, reducing operational costs, and further promoting the widespread application of geothermal energy in the heating sector.

Many scholars have conducted research on temperature control. For example, Markiewicz et al. proposed a framework to test centralized heating control algorithms and building heating system control algorithms, integrating information technology, artificial intelligence, machine learning, sensors, and Internet of Things (IoT) technologies, to control indoor temperature through evaluation indicators, seamless integration methods, and real-time performance monitoring mechanisms [8]. Machine learning algorithms are typically trained on historical data. For some sudden changes in heating systems, such as extreme weather causing abrupt changes in heat load or temporary modifications in building structure affecting heat distribution, the models may not adapt in time, leading to poorer temperature control in geothermal clean heating. Jeevadason et al. used Seebeck effect-based thermoelectric k sensors for temperature measurement, utilizing thermoelectric modules based on the reverse Seebeck effect to enhance the evaporation and condensation rates of TWSS

(Two-Wedge Solar Distiller), monitoring and controlling the yield of TWSS. A Temperature Control Unit (TCU) was developed to acquire data from temperature sensors and control the operation of thermoelectric modules, regulating device temperature [9]. Seebeck effect-based thermoelectric K sensors can measure temperature within a certain range; however, their accuracy is relatively low, with a general error of around ± 1~ ± 2.5℃ , which may lead to insufficient precision in temperature control. Hiraki et al. employed infrared sensors to measure surface temperature and validated the relationship between infrared sensor temperatures and various temperatures through CFD (Computational Fluid Dynamics) analysis, recreating the thermal environment of an office and controlling the office temperature [10]. CFD analysis is a method for simulating thermal environments based on mathematical models. However, this method is difficult to adapt effectively to the complex and variable working conditions of geothermal heating systems, resulting in poor control performance. Gao et al. established a reduced-order thermal capacity and thermal resistance model for the target building's heating, ventilation, and air conditioning systems. Subsequently, they designed a pipe-based MPC (Model Predictive Control) scheme to effectively manage the uncertainties of temperature in actual heating, ventilation, and air conditioning systems. By re-hypothesizing the predicted uncertain space within the pipes and incorporating actual temperature prediction errors, they achieved precise control of temperature [11]. However, this method does not adequately consider the precision of temperature monitoring, failing to accurately perceive subtle changes in temperature, leading to errors in control outcomes.

Fiber grating temperature sensors are based on the thermal-optical effect and thermal expansion effect of optical fibers [12], providing a high measurement accuracy that can precisely sense temperature changes, with errors controllable within a small range. This offers precise temperature data for geothermal heating systems [13], helping to maintain the indoor temperature within a comfortable range and avoid poor heating effects due to temperature errors. Moreover, these sensors are immune to electromagnetic interference, allowing them to operate stably in the complex electromagnetic environment of geothermal heating (such as those generated by devices like circulating pump motors and heat exchange station control cabinets), ensuring the accuracy and reliability of measurement data [14]. At the same time, fiber grating temperature sensors also have distributed measurement capabilities, allowing multiple gratings to be created on a single fiber, enabling simultaneous temperature measurements at various locations such as the geothermal well outlet, different positions in the heat exchange station, along the heating pipe network, and in all corners of the room. This makes the temperature distribution throughout the entire heating system clear, facilitating timely detection of temperature anomalies, whether it be excessive heat loss in the pipes or temperature being too high or too low in certain areas, all of which can be quickly monitored. Therefore, an intelligent control algorithm for geothermal clean heating temperature based on fiber grating temperature sensors is proposed, which can quickly and accurately adjust geothermal clean heating equipment to improve heating temperature. This article follows the technical route of temperature sensing network transmission intelligent control verification analysis, mainly including the following contents:

(1) Based on the thermal optical effect and thermal expansion effect of fiber Bragg grating, establish a linear relationship model between wavelength and temperature, and use fiber Bragg grating temperature sensors to achieve accurate temperature collection of geothermal clean heating systems;

(2) Constructing a distributed fiber Bragg grating temperature sensing network using time-division multiplexing technology to achieve real-time, synchronized collection and anti-interference transmission of temperature data from multiple locations in geothermal heating systems, including geothermal well outlets, heat exchange stations, pipe networks, and indoor areas;

(3) Taking the collected temperature data as input, the ITAE (time squared error absolute value integral) between the set temperature and the actual temperature is used as the control performance indicator. A BP neural network is designed to adaptively optimize the proportional, integral, and derivative parameters of the PID controller, forming the BP-PID intelligent control algorithm;

(4) Through anti-interference capability testing, step response comparison experiments with different control methods, and 24-hour indoor and outdoor temperature tracking monitoring, the superiority of the proposed algorithm is comprehensively verified from the dimensions of data packet transmission capability, overshoot, adjustment time, and temperature stability.

2 Intelligent Control Algorithm for Geothermal Clean Heating Temperature

2.1 Temperature Acquisition Based on Fiber Grating Temperature Sensors

Fiber Bragg Grating utilizes the photosensitivity of fiber materials to form a spatial phase grating in the fiber core through ultraviolet exposure. When broadband light is incident on the fiber grating, light at the wavelength satisfying the Fiber Bragg Grating will be reflected, while the remaining wavelengths will continue to transmit through the fiber grating. When external conditions such as temperature and stress around the grating change, the grating period or core refractive index will change, causing a shift in the central wavelength of the fiber grating. By detecting the shift in the grating wavelength, changes in the external environment can be obtained, as illustrated in Figure 1.

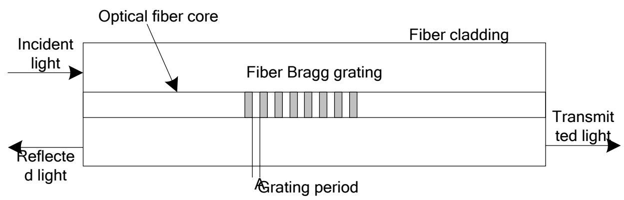

（a）Fiber grating structure

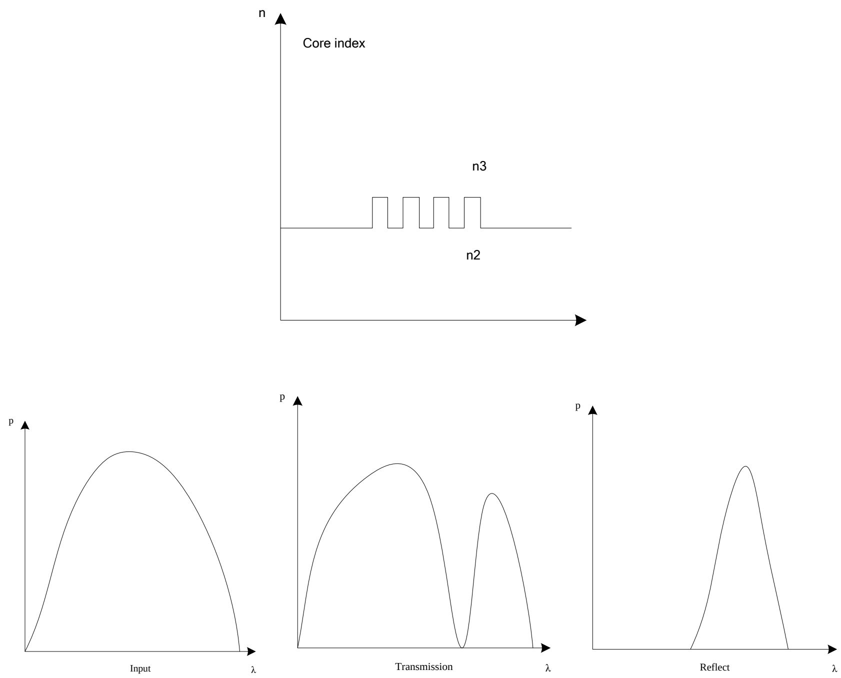

（b）Some parameters of fiber grating

Figure 1 Fiber grating sensor

Figure 1 (a) shows the basic structure of a fiber Bragg grating. After broadband incident light enters the fiber, only the light that satisfies the Bragg condition in the fiber grating region is reflected, while the rest of the light continues to propagate through transmission. The center wavelength of the reflection spectrum is determined by the grating period and the effective refractive index of the fiber core. Figure 1 (b) further illustrates the periodic distribution of the refractive index of the fiber core, where n1, n2, and n3 represent the refractive index changes at different positions. By detecting the drift of the reflected wavelength, changes in external temperature or strain can be inverted.

According to the coupled mode theory, the formula for the central reflection wavelength of the fiber grating is:

$$\lambda_B = 2n_{eff}\Lambda \quad (1)$$

Where, λ_B is the Bragg wavelength; n_{eff} is the effective refractive index in the fiber propagation mode; Λ is the fiber grating period.

The fiber grating temperature sensor utilizes the principle that changes in temperature will cause thermal expansion and the photo-thermal effect to alter the refractive index. The principle of temperature measurement using the fiber grating temperature sensor is illustrated in Figure 2.

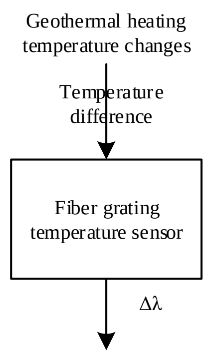

Figure 2 Temperature measurement by fiber grating temperature sensor

Figure 2 illustrates the process of converting temperature changes into wavelength drift using a fiber Bragg grating temperature sensor. The temperature change of geothermal heating causes a temperature difference in the environment where the sensor is located. Under the action of thermal expansion and thermal optical effects, the grating period and effective refractive index change, ultimately resulting in a drift of the Bragg center wavelength $\Delta\lambda_B$. By detecting this drift, temperature change information can be obtained.

In order to establish a quantitative relationship between wavelength drift and temperature changes, the Bragg condition (formula (1)) is differentiated with respect to temperature T. When the temperature changes ΔT, both the effective refractive index n_{eff} and the grating period Λ change. Therefore, it can be concluded that:

$$\frac{d\lambda_B}{dT} = 2\Lambda\frac{dn_{eff}}{dT} + n_{eff}\frac{d\Lambda}{dT} \quad (2)$$

The thermal optical coefficient ξ and thermal expansion coefficient α of fiber Bragg grating are defined as:

$$\xi = \frac{1}{n_{eff}} \frac{dn_{eff}}{dT} \quad (3)$$

$$\alpha = \frac{1}{\Lambda} \frac{d\Lambda}{dT} \quad (4)$$

By substituting formulas (3) and (4) into formula (2), we can organize and obtain:

$$\frac{d\lambda_B}{dT} = \lambda_B \left(\xi + \alpha \right) \quad (5)$$

Therefore, for a limited temperature change ΔT, the drift of the Bragg center wavelength $\Delta\lambda_B$ is:

$$\Delta\lambda_B = \lambda_B \left(\xi + \alpha \right) \Delta T \quad (6)$$

Further define the temperature sensitivity coefficient K_T of the fiber Bragg grating temperature sensor as:

$$K_T = \frac{\Delta\lambda_B}{\Delta T} = \lambda_B \left(\xi + \alpha \right) \quad (7)$$

According to formulas (6) and (7), there is a significant linear variation between temperature and wavelength. Based on the wavelength shift value, the change in the geothermal energy clean heating temperature state is determined, thereby determining the temperature. Although the fiber Bragg temperature sensor changes wavelength with temperature, due to the differences in temperature sensitivity and packaging processes of the fiber, it is necessary to calibrate the fiber Bragg temperature sensor. The wavelength-temperature relationship of the fiber Bragg sensor is determined in an adjustable temperature experimental chamber, as shown in Figure 3.

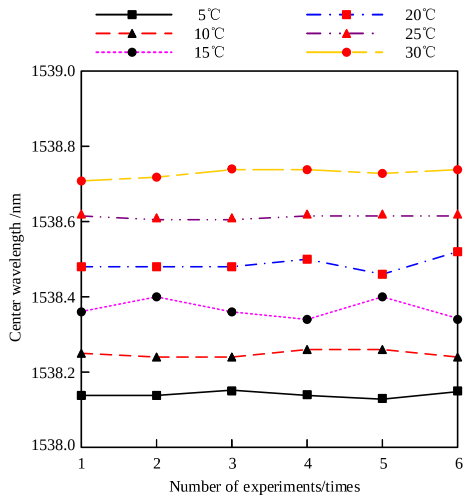

Figure 3 Wavelength-temperature relationship of fiber grating sensor

From Figure 3, it can be clearly observed that when the fiber Bragg temperature sensor is performing temperature measurement tasks, there is indeed a certain degree of fluctuation. It is worth noting that despite the fluctuations, the corresponding central wavelengths of these fluctuations are very close. Within the commonly used temperature range of 5 ℃ -30 ℃, for every 5 ℃ increase, the average center wavelengths of the fiber optic sensor are 1538.14nm, 1538.25nm, 1538.37nm, 1538.49nm, 1538.61nm, and 1538.72nm, respectively. Overall, this fluctuation is most likely caused by measurement errors or external interference. However, even with these fluctuations, they have minimal impact on the temperature measurement function of the fiber Bragg sensor. The reason is that the range of change in the central wavelength is very small, which can still reliably reflect the trend of temperature changes. Therefore, it can be seen that the fiber Bragg sensor performs excellently in temperature measurement and has a good temperature measurement effect. Its stable and reliable characteristics provide a solid and sufficient data guarantee for the precise control of geothermal energy clean heating using temperature data from the sensor in the subsequent stages. Based on this accurate temperature data, the heating control system can flexibly and efficiently adjust the heating strategy according to real-time temperature changes, thus ensuring the efficient operation of geothermal energy clean heating and the comfort and stability of the indoor environment.

To further quantitatively evaluate the linear response characteristics and measurement accuracy of FBG sensors, calibration experiments were conducted on the sensors. Figure 4 shows the temperature response curve of the FBG sensor, where each data point represents the wavelength mean of 6 repeated measurements at each temperature, and the error bar represents the measurement standard deviation. Linear fitting was performed on the mean point to obtain the fitting equation as $\lambda = 1538.02 + 0.0234 \times T$, with a sensitivity of 0.0234 nm/°C and a goodness of fit $R^2 = 0.9991$. The results indicate that the wavelength temperature relationship of FBG sensors has excellent linearity within the working temperature range of 5-30 ° C, providing a reliable sensing basis for precise temperature control of geothermal clean heating systems.

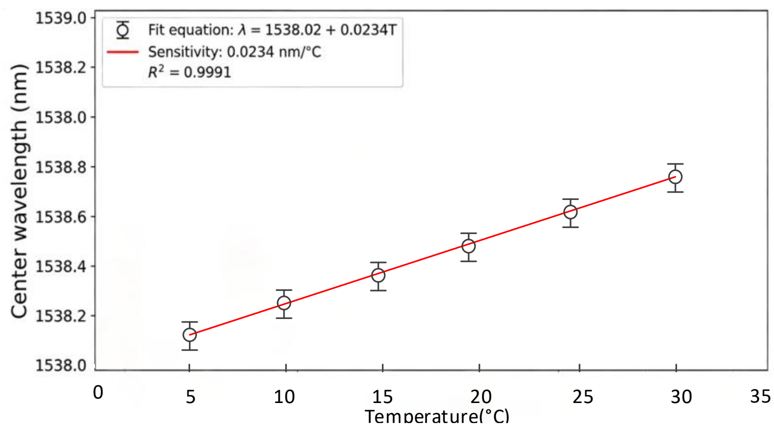

Figure 4 Temperature response curve of FBG sensor

2.2 Fiber Bragg Grating Sensor Network

The distributed fiber Bragg grating sensor network using TDM (time division multiplexing) achieves data transmission for geothermal clean heating temperature, as shown in Figure 5.

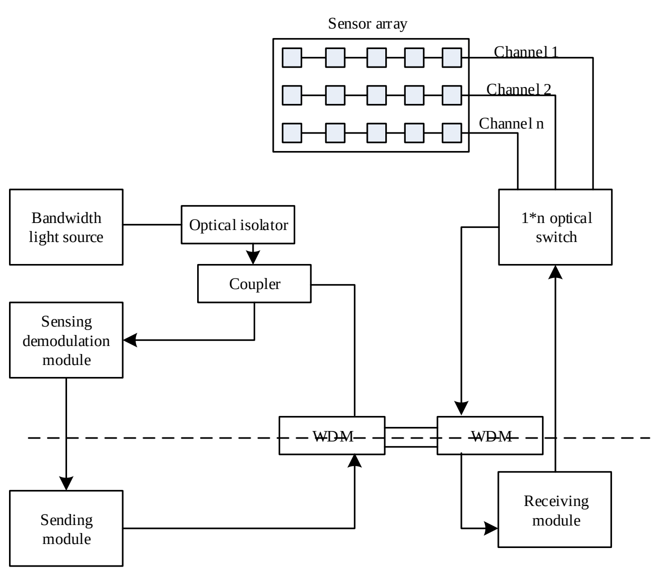

Figure 5 Structure of grating fiber sensing network

The dashed line in the figure divides the system into two parts: the part above the dashed line is the fiber Bragg grating sensing and demodulation part, referred to as the sensing part; the part below the dashed line is the sensing channel selection part connecting the control sensing channel queue and the demodulation module [15]. For the sensing part, the transmission optical fiber between the two WDM couplers connects the fiber Bragg grating temperature sensor array of the sensing network with the light source and the demodulation module. The upper right part of the figure is a multipoint sensor array, consisting of an optical switch $1\times n$ connected to n sensing channels forming the fiber Bragg grating temperature sensing channel queue, each of which is composed of multiple fiber Bragg grating sensing units. The upper left part is the light source and the fiber Bragg grating temperature sensing demodulation module, where the light source is connected to the fiber Bragg grating temperature sensing demodulation module through an optical coupler, with an optical isolator separating the broadband light source and the coupler. In order to enable the fiber Bragg grating temperature sensing demodulation module to communicate with multiple sensing channels in a TDM manner, the system includes a sensing channel selection part below the dashed line. Channel selection is collaboratively completed by the channel selection sending module located at the sensing demodulation end and the channel selection receiving module located at the sensor array end. The mechanism for selecting sensing channels is as follows: based on the control of the sensing demodulation module over the sensing channels, the channel selection sending module sends a sensing channel selection optical signal. This control signal is transmitted through optical fiber and received by the channel selection receiving module, which then controls the connectivity of each channel of the optical switch $1\times n$. Since the system uses different optical wavelengths for sensing and channel control, a WDM coupler is needed to complete the co-fiber transmission of the two wavelengths [16].

2.3 Intelligent Control of Geothermal Clean Heating Temperature Optimized by BP-PID

Using the collected temperature data as input, the intelligent control of geothermal clean heating temperature is developed. The PID controller is widely used in the field of automation control due to its simple structure and ease of control [17], achieving control through the deviation state of the controlled device. To enhance the ability of PID control over geothermal clean heating temperature, the control indicators are optimized and the PID controller is fine-tuned. In this process, a BP (Back Propagation) neural network is employed to select the proportional, integral, and derivative parameters of the PID controller. The BP neural network has powerful self-learning and adaptive capabilities, enabling it to automatically adjust the parameters of the PID controller according to the real-time operating conditions of the system, thus adapting to the complex and variable working conditions of the geothermal heating system. Consequently, the control ability of the PID controller is enhanced, making temperature control more flexible and efficient.

2.3.1 Selection of Performance Indicators for Geothermal Clean Heating Temperature Control

The performance metrics of the control algorithm can determine whether each metric of the system is in an optimal state. Generally, a perfect control system has optimal performance metrics; therefore, selecting reasonable performance metrics can effectively determine the control ability of the geothermal clean heating temperature control algorithm. Typically, the control results are mainly evaluated by the following performance metrics, namely the Integral of Absolute Error (IAE) and the Integral of Time multiplied by Absolute Error (ITAE).

The formula for the IAE metric is:

$$IAE = \int_0^{\infty} \left| e(t) \right| dt \quad (8)$$

In the formula, $e(t)$ represents the difference between the geothermal clean heating temperature input and output, t denotes the time, and the absolute value of $e(t)$ is integrated to obtain the value of this metric.

The IAE metric has a higher control capability for areas with small deviations, utilizing this metric to ensure that the system possesses high damping characteristics and transient response speed. However, when the control parameters are numerous, the variation range of this performance metric is small, making it unable to effectively adapt to situations where the system control parameters are variable. Therefore, this paper analyzes the ITAE metric, whose formula is:

$$ITAE = \int_0^{\infty} t \left| e(t) \right| dt \quad (9)$$

This indicator is obtained by multiplying the time t with the absolute value of the error. Using this metric as the performance indicator for geothermal clean heating temperature control can reduce the oscillation of the system’s temperature output under different output times while suppressing the errors that occur during the control process. Therefore, the ITAE is adopted as the performance metric for designing HVAC (Heating, Ventilation, and Air Conditioning) control systems.

2.3.2 Temperature Control Based on BP-PID

The specific process of PID controller controlling the clean heating temperature with geothermal energy is to transmit the real-time monitoring results of the clean heating temperature to the PID controller through the fiber grating temperature sensor network [18], and compare them with the set value $r(t)$, from this comparison, ITAE is obtained, and based on the situation of ITAE and the preset tuning parameters, a control signal is sent to control the geothermal heating equipment to change the temperature. The fiber grating temperature sensor network continuously acquires the temperature data of geothermal heating, repeating the above process to make the current temperature tend towards the set temperature value, thereby achieving the goal of stable output of clean heating temperature using geothermal energy. The structure of the PID control system is shown in Figure 6.

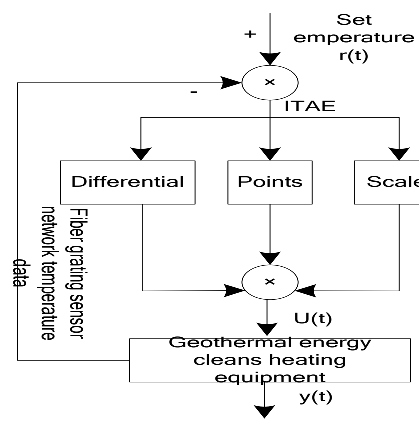

Figure 6 PID controller structure

As a linear control method, PID control can change by adjusting the PID coefficients. ITAE is the time multiplied by the absolute value of the error integral of the set value $r(t)$ and the output value $y(t)$. ITAE obtains the output value of the PID controller $U(t)$ under the superimposed effects of the proportional, integral, and derivative components of the controller.

The basic expression of the PID control law is:

$$U(t) = K_p \left[ITAE + K_i \int_0^t ITAEdt + K_d \frac{dITAE}{dt} \right] \quad (10)$$

Where: K_p is the proportional coefficient; K_i is the integral coefficient, $K_i = \frac{\Psi_i}{\Upsilon}$; K_d is the derivative coefficient; $K_d = \frac{\Psi_d}{\Upsilon}$, Ψ_i is the integral time constant; Ψ_d is the derivative time constant.

Due to the inability to adjust parameters in real-time online in traditional PID control systems [19], there is significant lag in the control system, resulting in long control times and low stability. Therefore, this control system introduces a backpropagation neural network structure based on traditional PID control, allowing real-time adjustments of PID parameters based on the deviation between the current temperature value and the set temperature value, thus achieving quick and stable attainment of the set value [20].

The specific way for BP neural network to adjust PID parameters in real time is as follows: in each control cycle, the input layer of BP neural network takes the current temperature deviation, the first-order difference of deviation, and the accumulation of deviation. After forward propagation, the three neurons in the output layer of the network correspond to the proportional coefficient Kp, integral coefficient Ki, and differential coefficient Kd of the PID controller. These parameters are transmitted in real-time to the PID controller for calculating the current control variable. At the same time, the system uses ITAE or error square integral as performance indicators, and updates the network weights in reverse through gradient descent method, making the next cycle's Kp, Ki, Kd more conducive to reducing temperature deviation. Through this structure, BP neural network can adjust PID parameters online and adaptively based on the current operating status and temperature error of the system, thus adapting to the complex and changing working conditions of geothermal heating systems, and improving the response speed and stability of temperature control.

The general topology structure of the BP neural network is shown in Figure 7. In the clean heating temperature control of geothermal energy, the BP neural network includes input layer, hidden layer, and output layer.

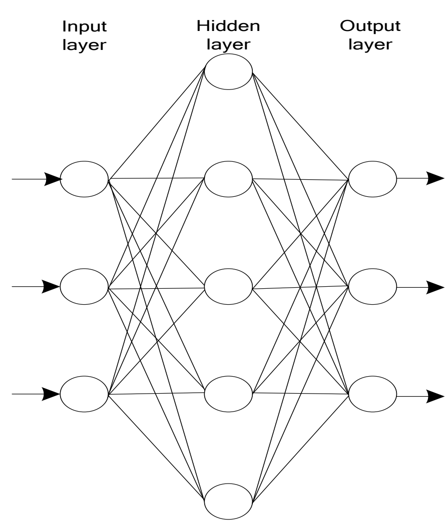

Figure 7 Topology structure of BP neural network

Taking the 3-layer BP neural network structure as an example, the output of the network input node is:

$$\Phi_j^{(1)} = X(j), (j = 1, 2, 3, \ldots, J) \quad (11)$$

The input and output of the network hidden layer are:

$$net_i^{(2)}(k) = \sum_{j=0}^{3} \omega_{ij}^{(2)} \Phi_j^{(1)} \quad (12)$$

$$\Phi_i^{(2)}(k) = f\left(net_i^{(2)}(k)\right), (i = 1, 2, 3, \ldots, I) \quad (13)$$

In the formula: $\omega_{ij}^{(2)}$ is the weighted coefficient of the hidden layer; the superscripts (1) and (2) represent the input layer and hidden layer, respectively; i and j are the number of nodes.

The activation function of the hidden layer neurons is the symmetric sigmoidal function:

$$f(x) = \frac{e^x - e^{-x}}{e^x + e^{-x}} \quad (14)$$

The input and output of the network output layer nodes are:

$$net_t^{(3)}(k) = \sum_{i=0}^{I} \omega_{li}^{(3)} \Phi_i^{(2)}(k) \quad (15)$$

$$\Phi_l^{(3)}(k) = g\left[net_l^{(3)}(k)\right], (l = 1, 2, 3, \cdots) \quad (16)$$

In the formula, ω_{li} is the weight coefficient of the output layer; $\Phi_1^{(3)}(k) = K_p$; $\Phi_2^{(3)}(k) = K_i$; $\Phi_3^{(3)}(k) = K_d$.

Since K_p , K_i , and K_d cannot be negative, the formula for the output layer neuron characteristic function $g(x)$ is:

$$g(x) = \frac{e^x}{e^x + e^{-x}} \quad (17)$$

Taking the performance index function as:

$$E(k)=\frac{\left(r_{in}(k)-y_{out}(k)\right)^2}{2} \quad (18)$$

In the formula: $r_{in}(k)$ is the input of the temperature control device; $y_{out}(k)$ is the output of the temperature control.

Using the gradient descent method to iteratively modify the weights of the neural network, so that the inertia term for fast convergence of the search is:

$$\Delta\omega_{li}^{(3)}(k)=-\mu\frac{\partial E(k)}{\partial\omega_{li}^{(3)}}+\alpha\Delta\omega_{li}^{(3)}(k-1) \quad (19)$$

In summary, substituting the updated weights of formula (19) into the above (12) to (16) completes the real-time adjustment of PID parameters, and combined with formula (10), derives the controller's output to achieve control over the geothermal energy clean heating temperature.

3 Experimental analysis

3.1 Experimental subjects

In order to verify the algorithm of this paper, a geothermal energy clean heating area is selected, and the geothermal energy clean heating equipment is shown in Figure 8 and the geothermal energy clean heating parameters are shown in Table 1. In the geothermal energy clean heating room set fiber grating temperature sensor to collect temperature data in the room, the sensor is shown in Figure 9.

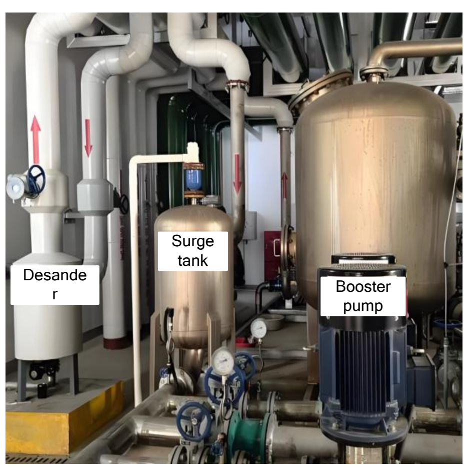

Figure 8 Geothermal energy cleaning heating equipment

Figure 7. Fiber grating temperature sensor

Table 1 Geothermal clean heating parameters

Stats	Argument
Number of heating units	1000
Geothermal water outlet temperature	80℃
Geothermal water return port	35℃
Heating hot water flow	1m3/h
Depth of geothermal well	2500m
Geothermal water pressure	1.2Mpa
Water yield of geothermal well	130m3/h
Heating system circulating pump power	12kw
Thermal efficiency of heat exchange station	93%
Heat loss rate of pipeline	7%
Utilization rate of geothermal energy	0.83
Co2 reduction compared with traditional heating	3.7t/ household per year

System cold start time	4.5h

To verify the effectiveness of the proposed algorithm, a time-division multiplexing (TDM) temperature sensing network based on fiber Bragg grating (FBG) was constructed, as shown in Figure 4. The network consists of 4 parallel sensing channels, which are selected through a 1 × 4 optical switch. Each sensing channel is connected in series with 5 FBG temperature sensors, for a total of 20 sensors. The center wavelengths of each sensor are located within the range of 1538 nm to 1539 nm and are distinguished through time-division multiplexing. The main component parameters are as follows: ASE broadband light source output power of 20 mW; FBG sensor 3 dB bandwidth of about 0.2 nm, reflectivity greater than 90%; The insertion loss of a 1 × 4 mechanical optical switch is less than 1.0 dB, and the switching time is less than 10 ms. The working wavelength of the WDM coupler sensing channel is 1535 nm~1565 nm, and the working wavelength of the control channel is 1310 nm, with an insertion loss of less than 0.8 dB. The isolation degree of the optical isolator is greater than 35 dB. The wavelength resolution of the FBG demodulator is 1 pm, the sampling frequency is 1 Hz, and the temperature measurement accuracy is ± 0.1 ℃; The transmission fiber adopts single-mode SMF-28. The sensor layout is as follows: one sensor is installed on the surface of the geothermal well outlet pipeline; Install one side entrance for the heat exchange station board replacement; Install one each in the indoor living room, bedroom, kitchen, and bathroom (1.5 meters above the ground); The remaining sensors are arranged at equal intervals along the outer wall of the heating main pipeline. The experimental room covers an area of 90 square meters, with insulation layers on the exterior walls and underfloor heating coils at the heating end. In the anti-interference ability test, an electromagnetic interference generator is used to apply different intensities of interference (1 V/m~10 V/m, 80 MHz~1 GHz) near the transmission cable, and the number of successfully transmitted data packets within 100 seconds under each interference level is monitored.

Based on the above settings, in order to verify the control effect of the proposed method, the control method based on wireless temperature sensor in literature [8], the temperature control method based on thermoelectric sensor and module in literature [9], and the model prediction control method in literature [11] are compared with the method of this paper for the control of the temperature of geothermal energy clean heating, and the control effect of each method is reflected by using the step response curves after control. In this way, the overshoot of each method is reflected, and the lower the overshoot is, the better the control effect is. To ensure the fairness and comparability of the experimental results, all comparison methods were tested on the same geothermal clean heating experimental platform. The experimental environment, heating equipment parameters (as shown in Table 1), temperature data source (all using real-time data from the same fiber Bragg grating temperature sensor network), set temperature (uniformly 25 ℃), sampling frequency, control cycle, and cold start state were all consistent. The comparative methods in references [8], [9], and [11] were configured according to the recommended parameters provided in their respective original texts, and pre tuned on this experimental platform to achieve their optimal control performance. The initial parameters of the PID controller were uniformly tuned using the Ziegler Nichols method. By setting the above control variables, all experimental conditions are completely the same except for the control algorithm itself, ensuring that the comparison results can truly reflect the differences in temperature control performance of each algorithm.

3.2 Analysis of experimental results

In order to verify the data transmission reliability of the TDM based fiber Bragg grating sensing network constructed in this article under electromagnetic interference environment, the following testing methods were designed. The application method and interference level definition of interference: using a programmable electromagnetic interference generator to apply electromagnetic interference of different intensities near the transmission cable of the fiber Bragg grating sensing network. The interference frequency scanning range is 80 MHz~1 GHz, covering the typical electromagnetic interference frequency bands generated by frequency converters, motors and other equipment in geothermal heating systems. Four interference levels are set, corresponding to applied electric field strengths of 3 V/m, 6 V/m, 10 V/m, and 15 V/m. At the same time, conduct baseline testing under interference free conditions as a reference for comparison. Measurement method for data transmission performance: In a sensing network, each fiber Bragg grating temperature sensor node sends data packets at a fixed frequency (1 Hz), each packet containing temperature measurement values and verification codes. At the receiving end, count the cumulative number of successfully transmitted data packets within a continuous 100 second time window. Each group of tests is repeated 3 times, and the average result is taken to draw a curve. The results are shown in Figure 10.

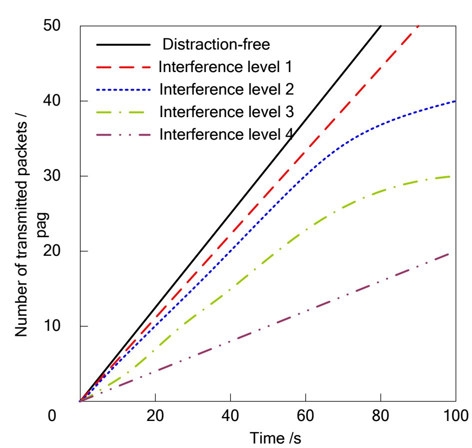

Figure 10 Anti-interference capability of fiber grating sensor network

Through Figure 10 can be seen that, based on TDM fiber grating sensing network has more excellent anti-interference ability, but what can not be avoided is that with the enhancement of the ability to interfere with the ability of data transmission will also be reduced, in the 1 level of interference on the sensing network is almost no effect, but to reach the 4 level and interference level of the strongest interference can be expected to be able to transmit the 20 packets of data through the 100s time. Although the number of transmitted packets decreases, the temperature control of the geothermal heating data can still be performed with 20 packets.

In order to verify the effect of the algorithm of this paper on the intelligent control of geothermal energy clean heating temperature, the control method based on wireless temperature sensors in the literature [8], the temperature control method based on thermoelectric sensors and modules in the literature [9], and the model prediction control method in the literature [11] are compared with the method of this paper for the temperature control of geothermal energy clean heating, and the step response curves are shown in Figure 11 after the control with different methods, and some of the parameters in the control process are shown in Table 2.

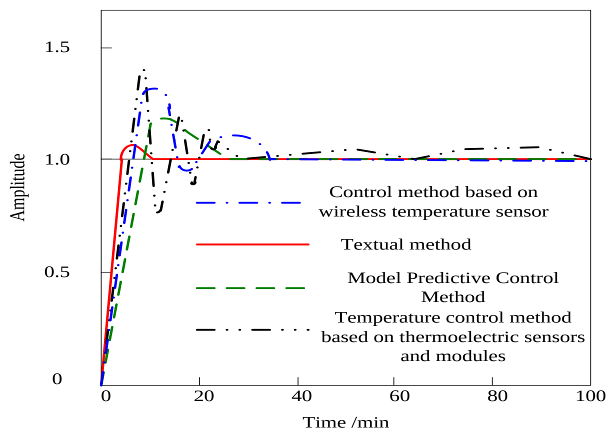

Figure 11 Step response results of different control methods

Table 2 The control effect of different control methods

Tuning parameter	Textual algorithm	Control method based on wireless temperature sensor	Model Predictive Control Method	Temperature control method based on thermoelectric sensors and

				modules
Overshoot /%	8	33	18	39
Adjust time /min	10.2	33	27	30
Holding time /s	90	67	73	24

Analyzing the data presented in Figure 10 and Table 2 in depth, the method proposed in this paper for geothermal energy clean heating control shows remarkable superiority compared with other algorithms. Firstly, we focus on the key index of overshooting, which is directly related to the magnitude of the indoor temperature exceeding the setpoint instantaneously when the heating system starts up or when the working conditions are switched, which has a significant impact on the comfort level. Using the temperature control method based on thermoelectric sensors and modules and the control method based on wireless temperature sensors, the overshooting amount is more than 30%, which means that the indoor temperature is very easy to fluctuate dramatically during the heating process, giving the user a bad experience of hot and cold, also reflecting the roughness of these two algorithms in response to the temperature regulation and control, and it is difficult to accurately grasp the rhythm of heat supply. Although the model predictive control method is slightly improved, the overshoot is reduced to 18%, but there is still a certain degree of temperature fluctuation potential problems. On the contrary, the algorithm in this paper, under its control, the overshooting amount is only 8%, this excellent performance shows its excellent control accuracy, can ensure the smooth operation of geothermal heating system with delicate regulation means, lock the indoor temperature in the appropriate zone, and create a constant and comfortable warm environment for the users. In addition, the adjustment time is also an important measure of the heating control system. In practical application scenarios, fast response and change of indoor temperature is essential to meet the immediate heating needs of users. In addition, when using the algorithm in this paper, it takes only 10.2 min to change the indoor temperature efficiently, so that the warmth can be delivered as quickly as lightning. In contrast, the wireless temperature sensor-based control method, the thermoelectric sensor and module-based temperature control method, and the model predictive control method are much slower and take about 30 min to achieve the same effect. This confirms the great advantage of this paper's algorithm in terms of efficiency. This is because the method in this article adopts a PID controller optimized by BP neural network. The BP neural network has strong self-learning and adaptive capabilities, and can dynamically adjust the proportional, integral, and derivative coefficients of the PID controller based on the real-time feedback ITAE index of the fiber Bragg grating temperature sensor network. When there is a sudden change in the thermal load of a geothermal heating system, neural networks can predict in advance and moderately reduce the proportional coefficient to avoid excessive heat output; When approaching the set temperature, enhance the integration effect to quickly eliminate steady-state errors; When the temperature change rate is too fast, introducing differential action to suppress fluctuations in advance. The mechanism that combines feedforward prediction with real-time correction achieves the best balance between fast response and smooth convergence in the system, resulting in lower overshoot and shorter adjustment time.

In order to verify the effect of this paper's algorithm for the intelligent control of geothermal energy clean heating temperature, the statistics of the room inside and outside the 24-hour temperature change, through the temperature changes in response to the temperature control effect of this paper's algorithm, the 24-hour indoor and outdoor temperature change is shown in Figure 12.

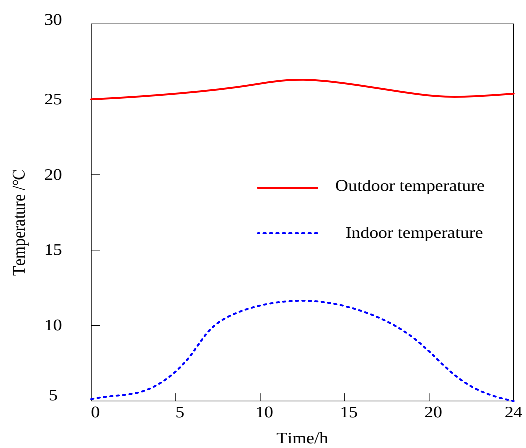

Figure 12 Temperature change in the room

By analyzing the indoor and outdoor temperature change curves in Figure 12, we can clearly understand the dynamics of temperature change throughout the day. At 5:00 a.m., with the sun gradually rising, the outdoor temperature begins to rise steadily, and reaches the peak of the day at 12-13:00 a.m., about 12 degrees Celsius, and then gradually decreases. On the contrary, the indoor temperature, under the effective control of the algorithm in this paper, is basically maintained at a comfortable and pleasant level of 25 degrees Celsius. Although the indoor temperature was affected to a certain extent by the sharp increase in outdoor temperature between 11 - 14 pm, there was a small fluctuation, but the fluctuation was so small that it was almost difficult to notice. From the actual feeling, this small temperature change basically will not let the human body produce obvious difference between hot and cold feeling. This excellent performance fully proves that the algorithm in this paper has strong temperature control capability. It can accurately sense the change of outdoor temperature, and quickly make corresponding adjustments to effectively resist the interference of external factors on the indoor temperature, so that the temperature in the room is always maintained at the optimal level of comfort, providing a stable and comfortable indoor environment for the people inside the room. The advantages of this algorithm in the application of geothermal energy clean heating system will undoubtedly greatly enhance the user experience and the operational efficiency of the heating system.

4 Conclusion

In response to the problem of large control overshoot caused by electromagnetic interference in traditional temperature sensors in geothermal clean heating systems, this paper constructs a fiber Bragg grating temperature sensing network based on time-division multiplexing (TDM), and uses BP neural network to optimize the proportional, integral, and derivative parameters of the PID controller in real time, forming an intelligent temperature control algorithm. The experimental results show that the sensor network can still stably transmit 20 data packets within 100 seconds in a strong electromagnetic interference environment (level 4 interference), effectively solving the problem of data distortion; At the same time, the proposed BP-PID control algorithm reduces the temperature overshoot to 8% and shortens the adjustment time to 10.2 minutes. In 24-hour dynamic testing, it can maintain the indoor temperature stable within the comfortable range of 25 ℃, significantly suppressing the disturbance caused by outdoor temperature fluctuations. The above results indicate that this method has clear engineering practical value for improving the control accuracy, operational stability, and user comfort of geothermal heating systems in cold regions. However, the validation of this study is based on a single geothermal system and specific operating conditions, and the generalization ability of the proposed algorithm in complex multi heat source coupled pipelines still needs further testing; In addition, the current deployment cost of fiber Bragg grating sensors is still higher than that of traditional electrical sensors, which may pose certain constraints on large-scale promotion. Future research will focus on reducing the cost of sensor networks, exploring economical solutions for wavelength division/time division hybrid multiplexing, and combining thermal load prediction models (such as Transformer and other deep learning methods) to achieve feedforward active control, in order to further enhance the algorithm's adaptability under dynamic conditions.

Fundings

1. Development and Reform Commission Project of Jilin Province : Key technology research and practice of shallow & medium deep geothermal heating in cold regions（2023C033-2）

2. Housing and Municipial and Rural Construction Hall Project of Jilin Province : Research on solar-ground source heat pump phase change heat storage heating system based on wind and solar power generation（2023-K-09）

3. Science and Technology Project of Educational Commission of Jilin Province：Research on control strategy of shallow & medium deep composite ground source heat pump system in cold regions（JJKH20251673KJ）

Conflicts of interest

There are no conflicts to declare.

Data availability

The datasets generated during and/or analysed during the current study are available from the corresponding author on reasonable request.

Author contributions

Shuang Li: conceptualization, data curation, formal analysis, investigation, writing-original draft. Lin Zhu: methodology, validation writing - review and editing. Yu Zhang: formal analysis, investigation, methodology. All authors commented on previous versions of the manuscript. All authors read and approved the final manuscript.

References

[1] Miocic JM, Schleichert L, Van d V AKR, Fast calculation of the technical shallow geothermal energy potential of large areas with a steady-state solution of the finite line source, Geothermics 116, 01 (2024).

[2] Dhaidan NS, Abbas HH, Rashid FL, Al-Mousawi FN, Al-Shohani WAM, Ameen A, et al., Enhancing the thermal performance of an agricultural solar greenhouse by geothermal energy using an earth-air heat exchanger system: a review, Geothermics 123, 01 (2024).

[3] Gkousis S, Welkenhuysen K, Harcout-Menou V, Pogacnik J, Laenen B, Compernolle T, Integrated geo-techno-economic and real options analysis of the decision to invest in a medium enthalpy deep geothermal heating plant. a case study in northern belgium, Energy Economics 134, 01 (2024).

[4] Dipippo R, Extraction turbines and feed-heating in geothermal binary plants: a thermodynamic performance assessment, Geothermics 116, 01 (2024).

[5] Ahmed AA, Assadi M, Kalantar A, Sliwa T, Aneta Sapińska-liwa, A critical review on the use of shallow geothermal energy systems for heating and cooling purposes, Energies 15, 01 (2022).

[6] Shin JH, Cho YH, A variable water flow rate control method of hybrid geothermal heat pump systems, Renewable Energy 226, 01 (2024).

[7] Abdenouri N, Zoukit A, Salhi I, Doubabi S, Model identification and fuzzy control of the temperature inside an active hybrid solar indirect dryer, Solar Energy 231, 328 (2022).

[8] Markiewicz M, Skaa A, Grela J, Janusz S, Stasiak T, Dominik Latoń, et al., The architecture for testing central heating control algorithms with feedback from wireless temperature sensors, Energies 16, 01 (2023).

[9] Jeevadason AW, Padmini S, Bharatiraja C, Enhancing freshwater productivity of twin wedge solar still by temperature control through thermoelectric sensors and modules, IEEE Sensors Journal 22, 9095 (2022).

[10] Hiraki T, Hiyama K, Omodaka Y, Murata K, Sekine K, Shichiri A, Estimation and control method of indoor thermal environment using next-generation human detection sensor, Journal of Environmental Engineering (Transactions of AIJ) 87, 335 (2022).

[11] Gao Y, Miyata S, Akashi Y, Energy saving and indoor temperature control for an office building using tube-based robust model predictive control, Applied Energy 341, 01 (2023).

[12] Anupam K, Akanksha M, Roli V, An axisymmetric metal and metal-oxide grating-structured self-reference fiber optic spr sensor, Journal of Optics 25, 01 (2023).

[13] Vaddadi VSCS, Parne SR, Vijeesh VP, Gandi S, Cenkeramaddi LR, Design and implementation of density sensor for liquids using fiber bragg grating sensor, IEEE Photonics Journal 14, 01 (2022).

[14] Dhanalakshmi S, Nandini P, Rakshit S, Rawat P, Narayanamoorthi R, Kumar R, et al., Fiber bragg grating sensor-based temperature monitoring of solar photovoltaic panels using machine learning algorithms, Optical Fiber Technology 69, 01 (2022).

[15] Byun H, Learning-based adaptive feedback control for tracking optimisation in wireless sensor actuator networking systems, IET Communications 16, 218 (2022).

[16] Anupam K, Akanksha M, Roli V, An axisymmetric metal and metal-oxide grating-structured self-reference fiber optic spr sensor, Journal of Optics 25, 01 (2023).

[17] Pastukhov VG, Maydanik YF, Temperature control of a heat source using a loop heat pipe integrated with a thermoelectric converter, International Journal of Thermal Sciences 184, 01 (2023).

[18] Mishra RK, Venkatesan S, Barpanda NK, An empirical study of waste heat re-utilization in thermal power plant using advanced fuzzy –pid technology, ECS Transactions 107, 9351 (2022).

[19] Taler D, Sobota T, Jaremkiewicz M, Taler J, Control of the temperature in the hot liquid tank by using a digital pid controller considering the random errors of the thermometer indications, Energy 239, 01 (2022).

[20] Begum KG, Coot bird optimization algorithm for the temperature control of continuous stirred tank reactor process, Asia-Pacific Journal of Chemical Engineering 18, 01 (2023).